IOP Conference Series: Earth and Environmental Science

PAPER • OPEN ACCESS

Sedimentation Analysis in Determining the Optimal Breakwater Layout for Grajagan Beach Fishing Port, Banyuwangi Regency

To cite this article: D T Laksono *et al* 2025 *IOP Conf. Ser.: Earth Environ. Sci.* **1473** 012004

Sedimentation Analysis in Determining the Optimal Breakwater Layout for Grajagan Beach Fishing Port, Banyuwangi Regency

D T Laksono[1], **V D Prasita**[2,3], **E A Kisnarti**[2,3], **R S Bintoro**[2,3]

[1] Master student of Marine Engineering, Faculty of Engineering and Marine Science, Hang Tuah University, Surabaya.
[2]Master of Marine Engineering, Faculty of Engineering and Ocean Sciences, Hang Tuah University, Surabaya.
[3]Program of Oceanography, Faculty of Engineering and Marine Science, Hang Tuah University, Surabaya.

E-mail: joelene.laksono@gmail.com

Abstract. Sedimentation that occurs in Grajagan Fishing Harbor, based on Google Earth images for the 2017-2023 time span tends to gather in the southern and eastern breakwater areas. The existence of sedimentation around the harbor can hinder fishing boat traffic. Sedimentation that occurs in the Grajagan Fishing Port area is thought to be less than optimal in the existing breakwater layout so that an optimal breakwater layout is needed. This study aims to determine the optimal breakwater layout based on hydro-oceanographic parameters using quantitative descriptive methods. The data used, namely: tidal, wind, wave, and sediment data. The data is used to analyze tidal patterns, wind and wave characteristics, current distribution patterns, and sediments. The results of the analysis are for determining the optimal breakwater layout. In Layout breakwater plan C sedimentation only occurs on the west side of the breakwater up to 0.6 m, while in the shipping channel and the berthing pond neither sedimentation nor erosion occurs. The simulation results of Layout breakwater plan A, B, and C, for Layout breakwater plan C is the most optimal and efficient in maintaining the berth pond for Grajagan Beach Fishing Port, Banyuwangi Regency.

1. Introduction

Sedimentation around the estuary is the result of the confluence of two water masses, namely sea water and fresh water [12]. Sediment deposition in estuaries occurs due to the interaction between tides, ocean waves, and current velocities that carry sediments [18]. Tides cause tidal currents that can move water masses, thus affecting suspense sediment transport and sediment concentration [10]. Ocean waves are a form of energy that can affect sediment transport in a body of water [2].

Sediment buildup results in sedimentation that can interfere with human activities on the coast, such as: Harbors and coastal defense buildings [6],[7]. One of them is port activities in the estuary to the shipping channel, due to siltation around the port. Activities in the port, such as being used as a place to lean ships with wide and deep river estuary conditions [17]. Shallow estuary conditions can cause obstruction to fishing boat traffic. In addition, the shallow condition of the estuary has an impact on the maximum size of the ship anchored in the port [8]. One of the ports located in the estuary is Grajagan Fishing Port, Banyuwangi Regency. Judging from google earth images, in the 2017-2023 timeframe sedimentation tends to gather in the area south and east of the breakwater.

Efforts to overcome the size limitations of anchored ships, one of which is by preventing siltation due to sedimentation around the port. Sedimentation prevention can be done by making sedimentation control buildings, such as breakwater. Breakwater is a structure that can reduce wave energy and function as a sediment barrier caused by ocean currents [9], [13]. Breakwater is effective in reducing sedimentation that occurs at the port location, because the supply of sediment from outside the breakwater can no longer enter the inner location of the port [1].

Meanwhile, breakwater construction has been carried out in Puger Waters. However, there is a problem of less than optimal layout of breakwater buildings in reducing high waves and restraining sediment transport. In this case, a re-planning of the breakwater layout was carried out [5], [19]. In addition, in the Fishing Port at IPP (Installation of Fishing Port) Pancer, Banyuwangi Regency, a breakwater evaluation was carried out due to the increasing sea wave pressure. This causes instability in the breakwater layout. In research [15]. In Grajagan Fishing Port, Banyuwangi Regency, the development of breakwater buildings in supporting the arrangement and development of the Port against the influence of waves. The influence factors of water conditions used, namely: waves and wind only [15].

Based on the above review, the author considers it necessary to conduct further research on the effectiveness of breakwater in reducing sedimentation. This research is in the Port area in the estuary, especially Grajagan Port, Banyuwangi Regency, which is still limited in research. This research was conducted to optimize the existing breakwater layout. In addition, hydro-oseanographic parameters as supporting parameters in the model simulation process. The results of this study can be used in an effort to consider decisions for the development of breakwater buildings in Grajagan Fishing Port, Banyuwangi Regency.

2. Methodology

Data collection was conducted in November 2023. The research site was situated within the Grajagan Coastal Fishing Port area in Banyuwangi Regency. The study area encompasses approximately 1,479,000 square meters surrounding the Grajagan PPP (Figure 1). A quantitative descriptive methodology was employed for this research.

2.1 Data

The data in this study consisted of primary and secondary data. Primary data used included sediment (sampling on November 20, 2023 which was divided into two, namely sediment load floating in the water and seabed samples), bathymetry (sounding on November 19, 2023 with an area of approximately 1,479,000 m2 using a Singlebeam Echosounder), and tides (taken from the BIG website for 30 days from November 1-30, 2023 and field observations for 3 days from November 19-21, 2023). Secondary data consisted of currents (taken from the Copernicus website during November 1-30, 2023 and field data for 26 hours on November 20, 2023 at 1 hour intervals), wind and waves (taken from the Copernicus website for 5 years from 2018-2022).

2.2 Processing

Data processing steps are carried out using several software, especially in simulating sediment distribution patterns using mike21 software. The following data processing is used:

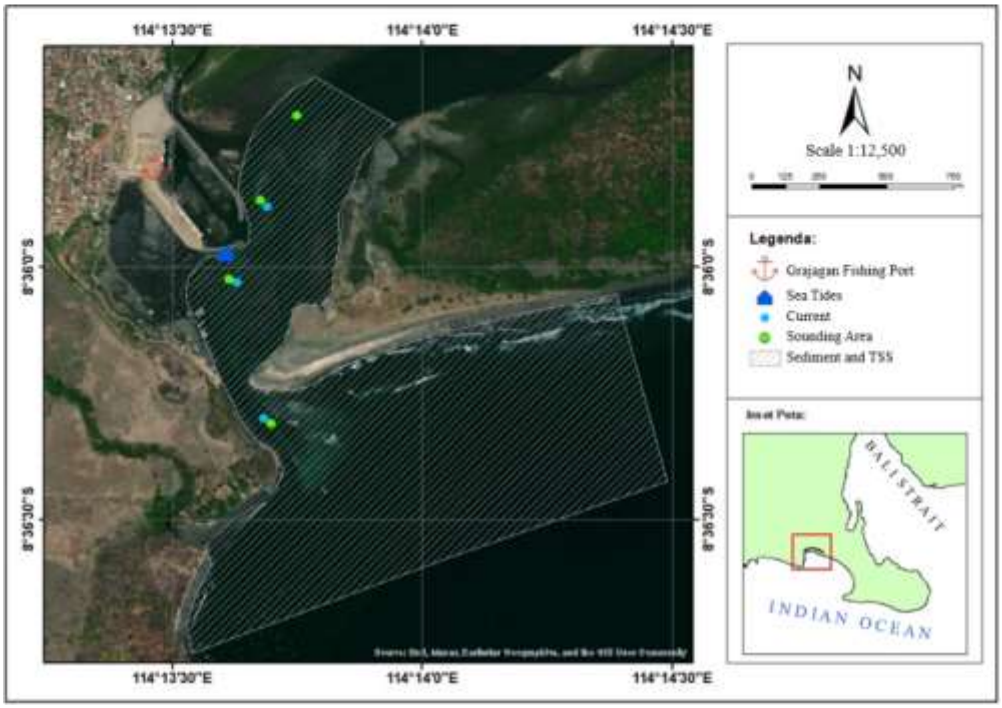

Figure 1. Sample observation point in Grajagan Waters, Banyuwangi.

2.2.1 Current

Current data in the form of direction and velocity will be separated into tidal currents and non-tidal currents by finding the u (east-west) and v (north-south) components. To get the u and v components, the following equation is used [14]:

a. Determines the u component by Cos direction multiplied by velocity.

$$u_{current} = v_{velocity}\ Cos\ \alpha \quad (1)$$

b. Determines the component of v by Sin direction multiplied by velocity.

$$v_{arus} = V_{\ velocity}\ Cos\ \alpha \quad (2)$$

c. Determine the tidal current component u, by the current component u minus the mean current u.

$$u_{tidal\ carrent} = u_{current} - u_{averange} \quad (3)$$

d. Determine the tidal current component v, with Current component v minus average current v.

$$v_{tidal\ carrent} = v_{carrent} - v_{averange} \quad (4)$$

e. Determine the direction of the tidal current:

$$\alpha_{tidal\ carrent} = Arctan\ (\frac{v_{tidal\ carrent}}{u_{tidal\ carrent}}) \quad (5)$$

f. Determine the speed of tidal currents:

$$Velocity_{\ tidal\ current} = \sqrt{(u_{tidal^2}) + (v_{tidal^2})} \quad (6)$$

g. Determine the direction of non-tidal currents:

$$\alpha_{arus\ non\ pasut} = Arctan\ (\frac{v_{arus\ rata-rata}}{u_{arus\ rata-rata}}) \quad (7)$$

h. Determine the speed of non-tidal currents:

$$Kec_{non-tidal\ current} = \sqrt{(u_{average^2}) + (v_{average^2})} \quad (8)$$

This flow data will also be used as model verification data in the Mike Zero application.

IOP Conf. Series: Earth and Environmental Science **1473** (2025) 012004 doi:10.1088/1755-1315/1473/1/012004

2.2.2 Sediment

Floating sediments will be processed using the SNI 06-6989-3-2004 method [3]. This method is used to determine the suspended sediment content. Seabed sediment samples are processed using the SNI 3423-2008 method [11]. This method is used to determine the type and size of sediment grains. The drifting sediment data will be used as verification of the sediment model at Mike Zero. Sediment grain size will later be used as model input data in the Mike Zero application.

2.2.3 Tidal

The tidal data is processed by descriptive statistics to obtain the values of the highest tide, lowest tide, and tidal stump. Tidal data in the form of water elevation will later be used as parameters in modeling.

2.2.4 Bathymetry

The sounding data is corrected with tidal values, after which a corrected depth value will be generated. Next, the corrected data was input to ArcGis 10.8 to layout the depth contour map. The corrected depth data is also used as a modeling parameter. Correction of sounding results to tides used the following formula [4].

$$D = (Z + TM) - (H - (y - Z_0)) \tag{9}$$

with:

D = corrected depth.
Z = depth measured by the echosounder.
TM = distance from the water surface to the transducer.
H = measured sea level height at time t.
y = average water level to zero palm.
Z_0 = the distance between the mean water level and the low tide level.

2.2.5 Wind and Wave

Wind and wave data will be visualized using the WR Plot application to produce wind rose and wave rose diagrams. Based on the wind and wave roses, the dominant wind direction and wave direction will be obtained. Wind data will later be used as input model data in the Mike Zero application.

2.3 Analysis

Data analysis includes: analysis of sediment distribution patterns and analysis of the feasibility of breakwater layouts. The analysis process starts from knowing the sediment distribution pattern, then making several new breakwater layouts. The breakwater layout was created in CAD software, then inputted into the boundary into Mike Zero software. The result is a model of sediment distribution patterns from several breakwater layouts, then scoring will be carried out to select the most optimal breakwater layout in preventing sedimentation.

3. Results and discussion

3.1 Tidal Conditions of Grajagan Harbor

Figure 2 shows the dynamic tidal fluctuations with MSL 0 (yellow color) from November 1-30, 2023. The highest tide (Figure 2) occurred on November 27 at 19:00 (134.5 cm) above mean high water level (MSL). The lowest tide occurred on November 28 at 02:00 with an elevation of -134.5 cm below MSL. The admiralty calculation results obtained a formzahl value of 0.69 with mixed tide predominant semidiurnal type 0.25 < F <= 1.5. Tidal data from BIG was used as modeling input in Mike21.

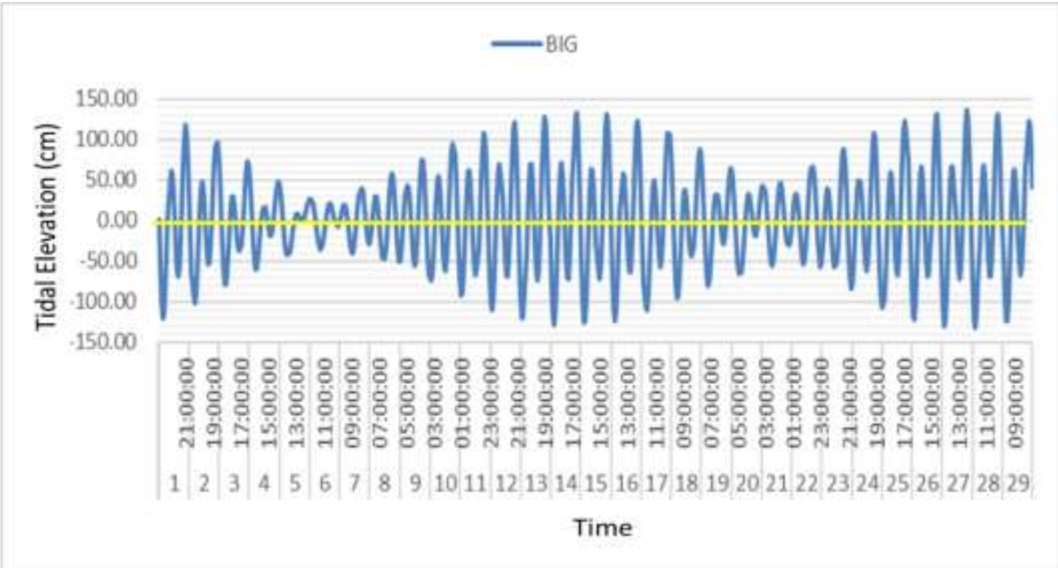

Figure 2. Tidal fluctuations of Grajagan Harbor for the period of November 1-30, 2023.

3.2 Bathymetry Conditions

The bathymetry profile in Figure 3, at the depth of the bottom of the estuary surface to the bottom of the sea surface has a depth value of 1.5 to -8.8m. The depth in the harbor basin area is quite shallow ranging from 1 to -1 m.

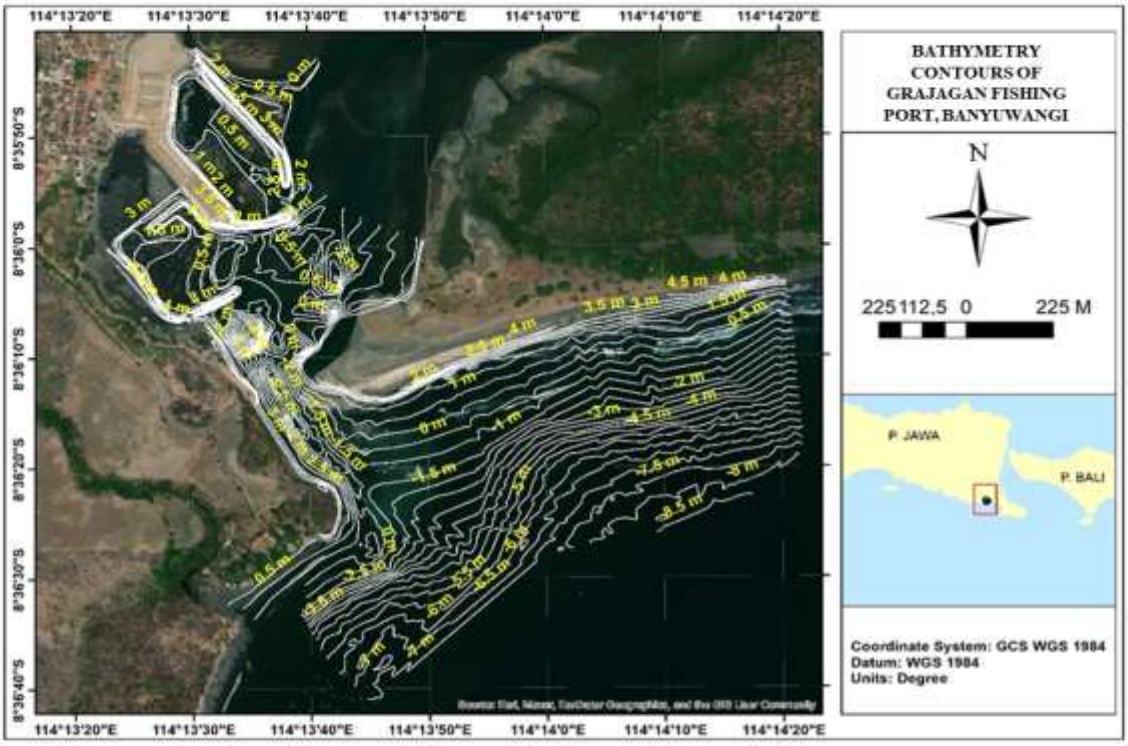

Figure 3. Bathymetry contours in Grajagan Waters.

3.3 Wave Conditions in Grajagan Waters

Wave data in Grajagan Waters was taken at https://marine.copernicus.eu with coordinates 8°40'0.01 "N and 114°15'0 "E for 5 years (2018-2022). On the fetch line, the effective fetch is determined according to the direction of the fetch line. The distance between fetch lines has a distance of 6o to the right and to the left. The fetch calculation map (Figure 4), determined by drawing a line from the shoreline towards the southeast, southwest and south.

On the map above the southeast fetch line is depicted in green, the southwest fetch line is depicted in red, the south fetch line is depicted in yellow. The southbound starting line is at 180˚, the southwest starting line is 225˚, and the southeast starting line is 135˚. The calculation of the effective fetch in the south direction results in 156.56 km. the southwest direction is 79.46 km, while for the southeast direction the result is 86 km. From the fetch calculation above, the waves are then calculated using the SPM (Shore Protection Manual) method.

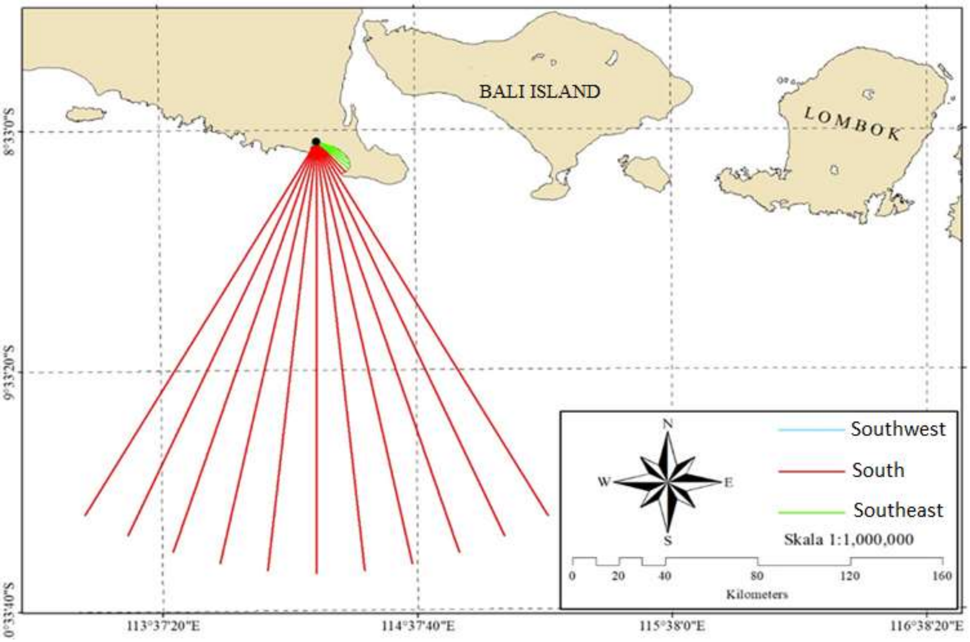

Figure 4. Fetch is effective.

Wind data processing (Figure 5a) shows that the wind pattern during the west season in the Grajagan area is dominated by winds blowing from the west. In the western season, the wind speed is between 0-9 m/s, while the wave height ranges from 0-1.50 m. The dominant wind blows (3-6 m/s) with a frequency of 43.5 %, while the wave height is dominated by the range of 0-0.30 m with a frequency of 86.5 %. This wind data if classified using the Beaufort Scale then the dominant wind during the western season in the Grajagan area is included in the weak wind category (0.3-1.5 m/s). The wave height category if classified using the BMKG Wave category then falls into the calm category (0.1 m-0.5 m).

Figure 5b shows that the wind pattern during transitional season 1 is dominated by winds blowing from the east. In transitional season 1, wind speeds ranged from 0-9 m/s, while wave heights ranged from 0-1.5m. The dominant wind blew (3-6 m/s) with a frequency of 53.3 %, while the dominant wave height ranged from 0-0.3 m with a frequency of 63.0 %. If this wind data is classified using the Beaufort Scale, the dominant wind during transitional season 1 in the Grajagan area is categorized as gentle and moderate breeze (3.4-7.9 m/s). Then, for the wave height category if classified using the BMKG Wave category, it is included in the calm category (0.1 - 0.5 m).

Wind patterns during the eastern season (Figure 5c) in the Grajagan area are dominated by winds blowing from the southeast. In the eastern season, the wind speed ranges from 0-9 m/s, while the wave height is between 0-1.50 m. The dominant wind blows at 3-6 m/s with a frequency of 69.3 % and the dominant wave height ranges from 0-0.3 m with a frequency of 26.7 %.

The wind pattern during transitional season 2 in the Grajakan area (Figure 5d) is dominated by winds blowing from the southeast. During transitional season 2, wind speeds ranged from 0-9 m/s, while wave heights ranged from 0-1.5m. The dominant wind blows with a speed of 3-6 m/s and a frequency of 53.6 %. Wave height is dominated by the height range of 0-0.3 m with a frequency of 40.2 %. On the Beaufort Scale, the transitional season 2 wind data is categorized as gentle and moderate breeze (3.4-7.9 m/s). Transitional season 2 wave heights are categorized as calm (0.1-0.5 m) when classified according to the BMKG wave height category.

The characteristics of significant wave height (Hs) during the western season show a significant level of variation. Based on the graph of Hs height and period in Figure 6a, that throughout the western season for a period of 5 years, namely in 2018-2022 has Hs height with a range of 0.05-0.85 m and a period ranging from 0.31-4.96 s. Significant waves are a statistical measure that reflects the average height of the largest waves in a particular area. In the western season conditions that took place in 2018-2022, the highest Hs values were in 2018 (0.27 m), 2019 (0.85 m), 2020 (0.58 m), 2021 (0.24 m), and 2022 (0.24 m). Wave period measures the time interval between two consecutive peaks or two consecutive valleys of ocean waves. The highest period values in the western season were recorded in 2018 (2.39 s), 2019 (4.96 s), 2020 (4.35 s), 2021 (1.92 s), and 2022 (1.95 s). Wave period can vary depending on a number of factors, including wind speed and duration, distance traveled by the wind, and water depth.

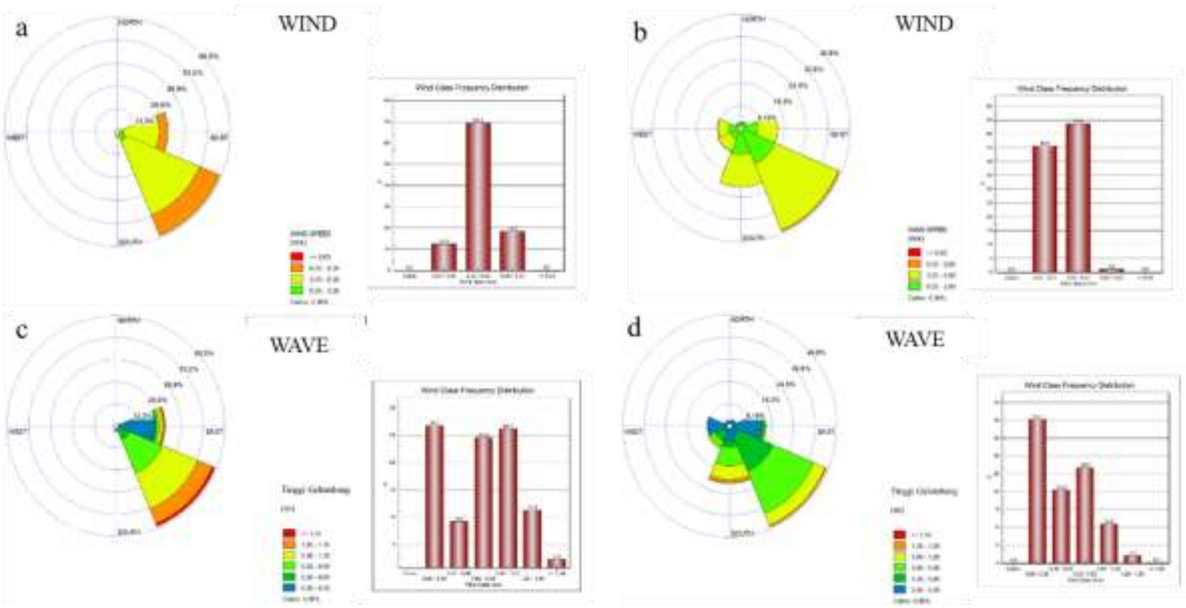

Figure 5. Wind and wave distribution of (a) west monsoon, (b) transition season 1, (c) east monsoon, and (d) transition season 2.

The height of Hs during transitional season 1 shows a significant level of variation, based on the height and period of Hs (Figure 6b). During transitional season 1 in the 5-year period of 2018-2022, Hs ranged from 0.72-1.16 m (2.81-5.46 s). During transitional season 1 which took place in 2018-2022, the highest Hs values were in 2018 (1.16 m), 2019 (1.18 m), 2020 (1 m), 2021 (0.97 m), and 2022 (0.43 m). In addition, the highest period values in transitional season 1 were recorded in 2018 (5.43 s), 2019 (5.46 s), 2020 (5.1 s), 2021 (5.1 s), and 2022 (3.81 s).

The characteristics of high Hs during the eastern season show a significant level of variation. Based on the graph of Hs height and period (Figure 6c), during the eastern season that took place in the period 2018-2022, Hs height ranged from 0.9-1.42 m (4.67-5.82 s). In the eastern season conditions that took place in 2018-2022, the highest Hs values were in 2018 (1.23 m), 2019 (1.08 m), 2020 (1.42

IOP Conf. Series: Earth and Environmental Science **1473** (2025) 012004 doi:10.1088/1755-1315/1473/1/012004

m), 2021 (1.2 m), and 2022 (1.25 m). The highest period values in the eastern season were recorded in 2018 (5.54 s), 2019 (5.31 s), 2020 (5.82 s), 2021 (5.51 s), and 2022 (5.56 s). The characteristics of Hs height during transition season 2 show a significant degree of variation. Based on the height and period of Hs (Figure 6d), for 5 years (2018-2022), the resulting Hs height ranged from 0.54-0.96 m with a period of 4.08-5.41 s. In the conditions of transitional season 2 (Figure 5d) lasting in 2018-2022, the highest Hs values were in 2018 (0.94 m), 2019 (0.81 m), 2020 (0.96 m), 2021 (0.96 m), and 2022 (0.84 m). The highest period values in transitional season 2 were recorded in 2018 (5.41 s), 2019 (5.06 s), 2020 (5.14 s), 2021 (5.52 s), and 2022 (5.05 s).

Based on Figure 7, shows the condition of the direction and speed of the current against the tide. When heading towards the tide, the dominant tidal current conditions move towards land, with speeds ranging from 0.04-0.14 m/s, then when heading towards the ebb current conditions have a fairly high speed value with a range of 0.05-0.28 m/s. The direction of the tidal current when heading to low tide, the current moves away from land. When the lowest tide and the highest tide the direction of the tidal current tends to turn and move towards the opposite direction. The condition of tidal current velocity at the lowest ebb and highest tide has a small speed value.

3.4 Tidal Current Conditions

At high tide (Figure 9b), the current speed at sea ranges from 0 to 0.095 m/s with the dominant direction towards land. At the coast, the current speed is very low, ranging from 0 to 0.24 m/s, with the current direction following along the coastline. At the mouth of the river, the current speed increases to 0.012 m/s to 0.085 m/s, indicating a stronger flow as the water movement starts to be affected by the tide. In the anchorage area, the current speed ranges from 0 to 0.035 m/s with the dominant direction towards land.

- *Existing Tidal Flow Conditions*

At the lowest ebb (Figure 8a), current velocities in the berth pond ranged from 0-0.035 m/s with the dominant direction towards the sea, indicating a fairly calm current as water flows out of the harbor area. At the estuary, current velocities ranged from 0.015-0.060 m/s, indicating more moderate water movement. On the coast, the current speed is very low, ranging from 0-0.020 m/s with the current direction away from land. Meanwhile, in the open sea, the current speed ranged from 0-0.080 m/s, indicating stronger currents in the open sea during the lowest low tide period.

During the ebb tide (Figure 8b), the current speed in the sea ranged from 0-0.04 m/s (dominant direction towards land). Along the coast, the current speed is very low (0-0.030 m/s), with the current direction still towards land. At the mouth of the river the current speed increases to 0.02 m/s-0.14 m/s, which indicates a stronger flow because the water movement is affected by the tide. The current speed at the mouth of the river increased due to the narrowing of the estuary. In the anchorage pond, the current velocity decreased (0-0.045 m/s) with the dominant direction towards land.

At the highest tide (Figure 8c), the current speed in the anchorage pond ranged from 0-0.050 m/s (dominant direction towards land), indicating a rather calm current as the water started to enter the harbor area. At the estuary, current velocities reached 0.020-0.095 m/s, indicating a more moderate flow of water towards land. Along the coast, the current speed ranges from 0-0.040 m/s, indicating an increased volume of water flowing towards the shore. In the open sea, current speeds ranged from 0-0.110 m/s, indicating stronger currents in the open sea during the highest tide period.

Figure 8d shows the tidal current when heading towards low tide, the current speed in the dock pond ranges from 0-0.040 m/s (dominant direction towards the sea). This condition indicates that the water begins to move out of the anchorage pond towards the sea along with the low tide. At the estuary, the current speed increases to 0.010-0.2 m/s, indicating stronger water flow as it approaches the sea. Along the coast, the current speed ranges from 0-0.025 m/s (the direction of the current is still away from land). Meanwhile, in the open sea, the current speed ranges from 0-0.02 m/s with the dominant direction towards the sea. This condition indicates a stronger current when the water moves away from land during the period towards low tide. This current pattern shows the movement of water generally out of the land towards the sea during this period.

- *Tidal Current Conditions Breakwater Plan A*

At the lowest ebb (Figure 9a), the current velocity in the berth pond is 0-0.02 m/s (dominant direction towards the sea), indicating a fairly calm current as the water flows out of the harbor area. At the estuary, the current speed is 0.015-0.055 m/s, indicating more moderate water movement. On the coast, the current speed is a very low 00.018 m/s (current direction away from land). Meanwhile, in the open sea, the current speed was 0-0.070 m/s, indicating stronger currents in the open sea during the lowest low tide period.

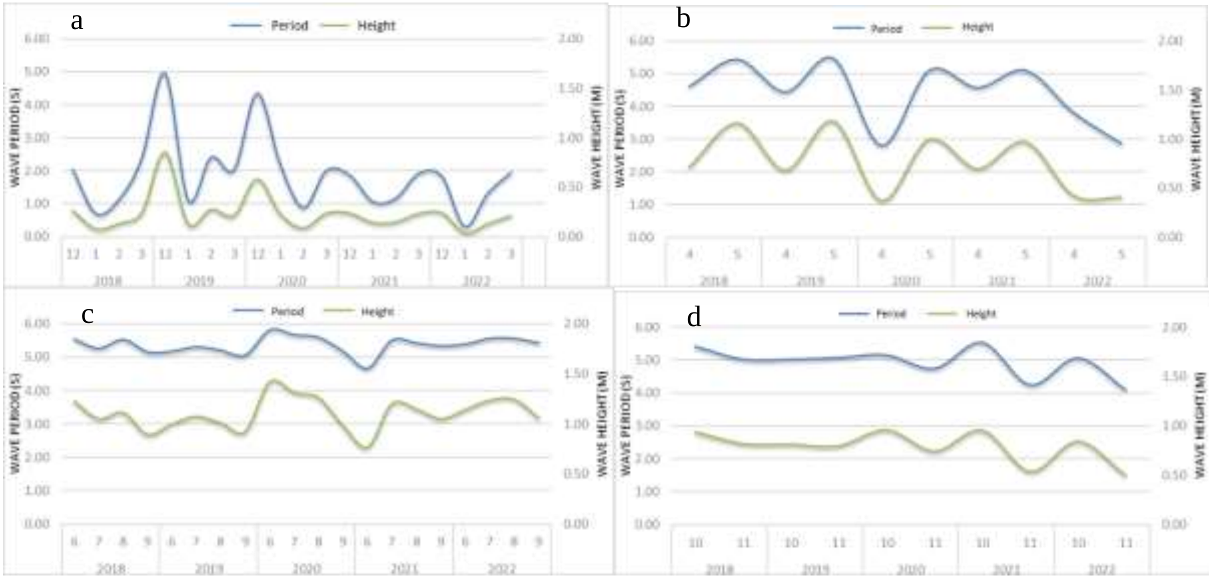

Figure 6. Significant wave height and period of (a) western season, (b) transitional season 1, (c) eastern season, and (d) transitional season 2.

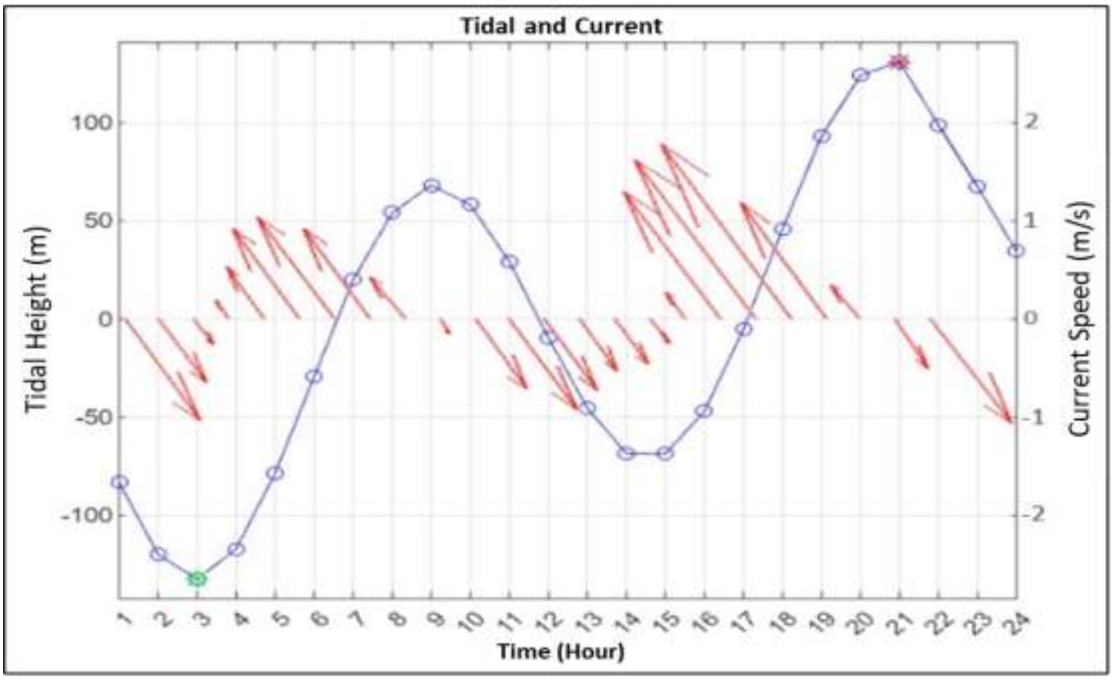

Figure 7. *Featherplot of water level, current velocity and direction November 28, 2023.*

In Figure 9c during the highest tide, the current velocity in the anchorage pond ranges from 0-0.045 m/s with the dominant direction towards land, indicating a rather calm current as the water begins to enter into the harbor area. At the estuary, the current speed is 0.018-0.090 m/s, indicating a more moderate flow of water towards land. Along the coast, current velocities ranged from 0-0.035 m/s, indicating an increased volume of water flowing towards the shore. In the open sea, current velocities ranged from 0-0.105 m/s, indicating stronger currents in the open sea during the highest tide period.

During low tide (Figure 9d), the current speed in the berth pond is between 0-0.030 m/s with the dominant direction towards the sea. Water begins to move out of the anchorage pond towards the sea as the tide recedes. At the estuary, the current speed increases to 0.02 m/s-0.24 m/s, indicating stronger water flow as it approaches the sea. Along the coast, the current speed is 0-0.020 m/s, with the current direction still away from land. In the open sea, the current speed is 0-0.090 m/s with the dominant direction towards the sea, indicating stronger currents as the water moves away from land during the period towards low tide. The decrease in current velocity in the berth pond was influenced by the tide beginning to move water out of the harbor area.

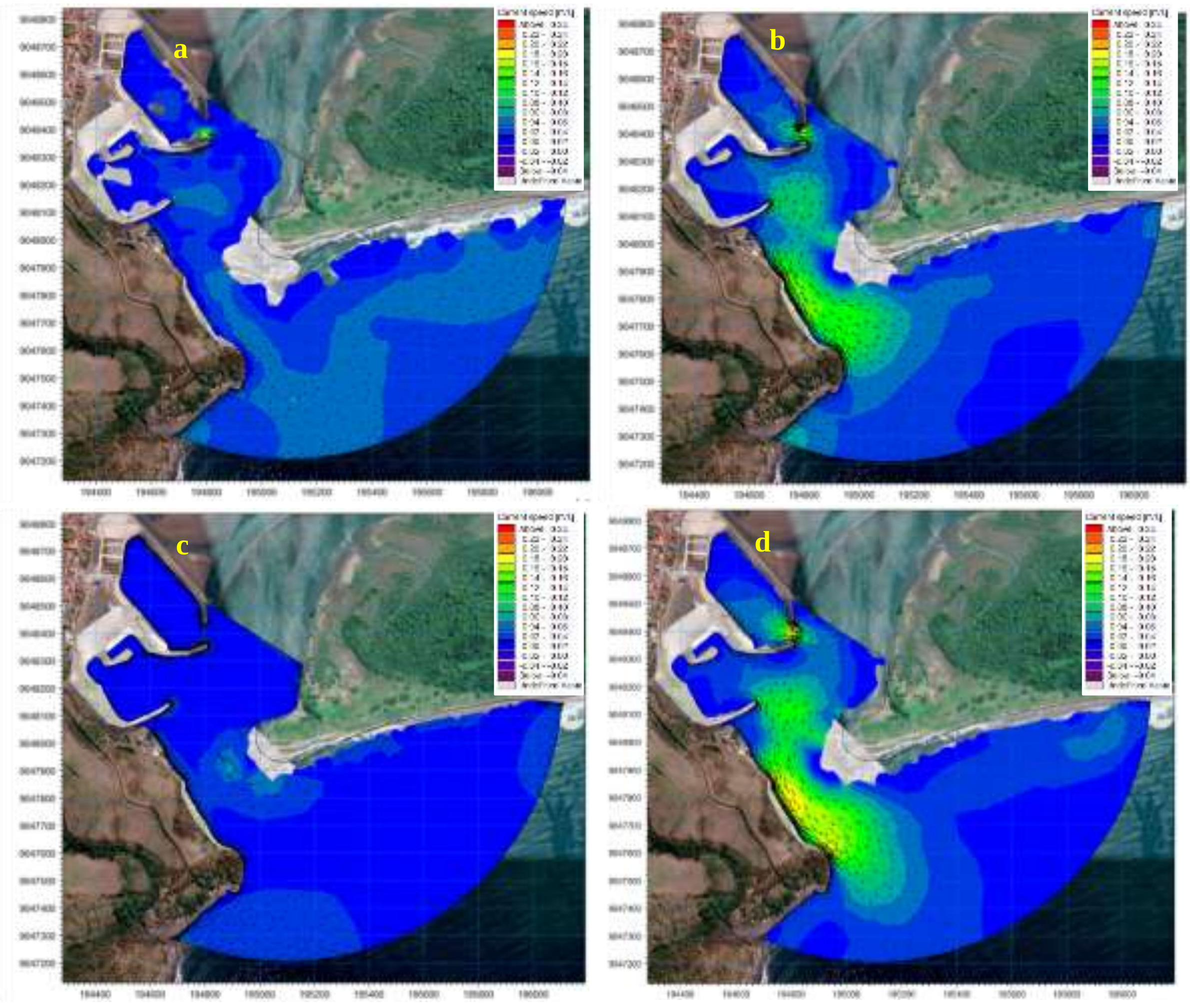

Figure 8. Tidal currents at (a) lowest ebb, (b) towards high tide, (c) highest tide, and (d) towards low tide.

- *Tidal Current Condition of Breakwater Plan B*

At the lowest ebb (Figure 10a), the current speed in the berth pond was 0-0.020 m/s with the dominant direction towards the sea, indicating a fairly calm current as the water flows out of the harbor area. At the estuary, the current speed ranges from 0.010-0.04 m/s, indicating calmer water movement. On the coast, the current speed is very low, between 0-0.015 m/s with the current direction away from land. Meanwhile, in the open sea, the current speed ranged from 0-0.070 m/s, indicating stronger currents in the open sea during the lowest low tide period.

During the ebb tide (Figure 10b), the current speed at sea is 0-0.085 m/s with the dominant direction towards land. At the coast, the current speed is very low, between 0-0.022 m/s, with the current direction still towards land. At the estuary, the current speed increases to 0.02-0.16 m/s, indicating a stronger flow due to the movement of water that is starting to be affected by the tide. In the dock pond, the current speed ranged from 0-0.030 m/s with the dominant direction towards land. The decrease in current velocity in the anchorage pond is influenced by the presence of a breakwater that makes the waters calmer.

The tidal currents during the highest tide (Figure 10c), showing current velocities in the anchorage pond ranging from 0-0.04 m/s with a dominant direction towards land, indicate that the currents tend to calm down as the water begins to enter the anchorage pond during the highest tide period. At the estuary, the current speed reaches 0.02-0.04 m/s, indicating a calmer flow of water towards land. Along the coast, the current speed ranges from 0-0.04 m/s, indicating an increased volume of water flowing towards the shore. In the open sea, the current speed is still relatively calm between 0-0.04 m/s.

The current velocity in the berth pond ranged from 0-0.035 m/s with the dominant direction towards the sea. This indicates that water begins to move out of the anchorage pond towards the sea as the tide recedes (Figure 10d). At the mouth of the river, the current speed increases to 0.012-0.075 m/s, indicating stronger water flow as it approaches the sea. Along the coast, the current speed ranges from 0-0.020 m/s, with the current direction still away from land. Meanwhile, in the open sea, the current speed ranges from 0-0.090 m/s with the dominant direction towards the sea, indicating stronger currents as the water moves away from land during the period towards low tide.

- *Tidal Current Condition of Breakwater Paln C*

During the lowest tides (Figure 11a), the current speed in the anchorage pond is 0-0.020 m/s with the dominant direction towards the sea. At the estuary, the current speed increases to 0.012-0.050 m/s, indicating a stronger flow of water towards the sea. On the coast, the current speed is very low, ranging from 0-0.015 m/s with the current direction away from land. In the open sea, the current speed is 0-0.065 m/s, indicating a stronger current with the dominant direction towards the sea. This shows the current pattern moving away from land during the lowest low tide period.

At high tide (Figure 11b), the current speed at sea is 0-0.085 m/s with the dominant direction towards land. On the coast, the current speed is very low, 0-0.022 m/s, with the current direction still towards land. When at the mouth of the river the current speed increases to 0.010-0.14 m/s, this is due to the movement of water that begins to be affected by the tide. In the anchorage pond, the current speed is 0-0.030 m/s with the dominant direction towards land. The decrease in current velocity in the anchorage pond is influenced by the presence of a breakwater that makes the pond waters calmer.

The tidal current during the highest tide (Figure 11c), has a speed of 0-0.048 m/s in the dock pond with the dominant direction towards land. This indicates that the current tends to calm down as the water begins to enter the anchorage pond during the highest tide period. At the mouth of the river, the current speed reached 0.020-0.100 m/s, indicating a more moderate flow of water towards land. Along the coast, current velocities range from 0-0.042 m/s, indicating an increased volume of water flowing towards the shore. In the open sea, current velocities ranged from 0-0.04 m/s, indicating still currents in the open sea during the highest tide period.

During the ebb tide (Figure 11d), the current speed in the dock pond is 0-0.035 m/s with the dominant direction towards the sea. This condition indicates that the water begins to move out of the anchorage pond towards the sea along with the ebb. At the estuary, the current speed increases to 0.02-0.2 m/s, indicating stronger water flow as it approaches the sea. Along the coast, the current speed ranges from 0-0.020 m/s, with the current direction still away from land. Meanwhile, in the open sea, the current speed ranges from 0-0.090 m/s with the dominant direction towards the sea, indicating stronger currents as the water moves away from land during the period towards low tide.

3.5 Model Validation

Tidal data validation was conducted by comparing field data with BIG data that had been simulated in Mike21 (Figure 12). The MSL from the BIG data is equalized with the field data which is 0 cm. Figure IV.29 shows the same daily tidal cycle. Based on the field data, the highest tidal surge occurred on November 19 at 00:00 with the highest water level 50 cm above MSL and the lowest tidal surge occurred with the lowest water level -50 cm below MSL on November 20 at 06:00. Meanwhile, based on the model results, the highest tidal ridge occurred on November 19 at 00:00 with the highest water level of 61 cm above MSL and the lowest tidal ridge occurred on November 19 at 05:00 with the lowest water level of -81 cm below MSL.

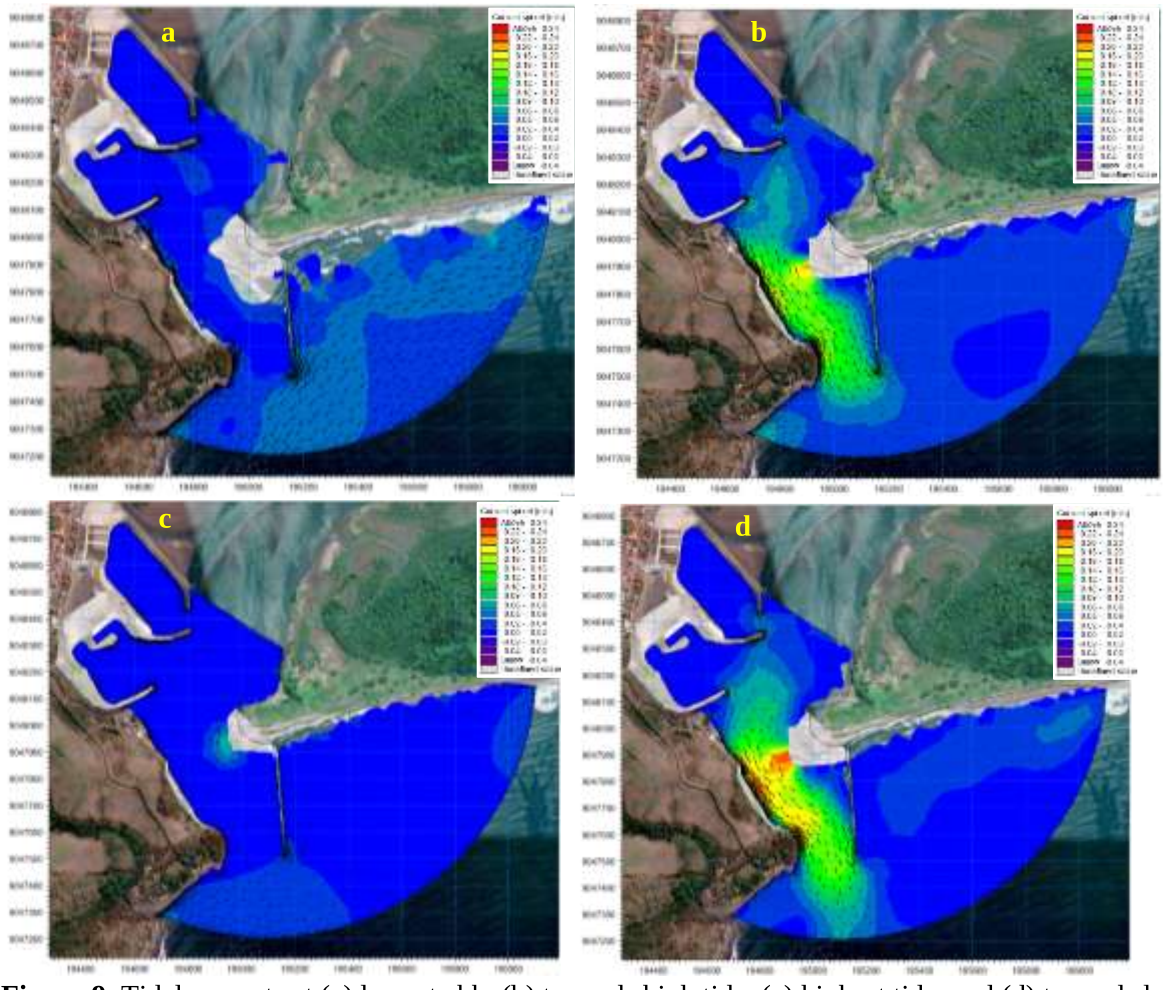

Figure 9. Tidal currents at (a) lowest ebb, (b) towards high tide, (c) highest tide, and (d) towards low tide.

3.6 Sediment Conditions

3.6.1 Sediment Condition Before Breakwater

Figure 13a during the initial condition, there is no difference in elevation because it is an existing condition before being affected by tidal currents. In the initial condition, the elevation value still follows the depth value during the survey. Elevation conditions on the estuary side of the river range from 0 to -3.2 m, the harbor area ranges from 0-1.6 m, and on the beach area ranges from 0-3.2 m. The final bed level condition of Figure 13b, has varying depths. The estuary area experienced erosion with bed level values ranging from -0.8 to -3.2m. The bed level condition in the harbor area has sedimentation of up to 1.6m. The sediment comes from the coast to the harbor area directly.

Erosion events occurred at the estuary, beach area and the inner side of the harbor which can be seen in Figure 13c. In the estuary area, erosion of 0 to -0.3 m occurred, while the western side of the estuary experienced erosion of up to -1 m. Then. The waters along the shoreline also experienced erosion up to -0.75 m. In addition to erosion events, sedimentation also occurred in the harbor basin area by 0-1 m, while the inner side of the northern area of the harbor experienced erosion up to -0.9 m. In the coastal area, erosion occurs due to rip currents that carry sediment to the sea, while sedimentation that occurs in the harbor basin is due to longshore currents that carry sediment from along the coastline to the estuary and into the harbor basin.

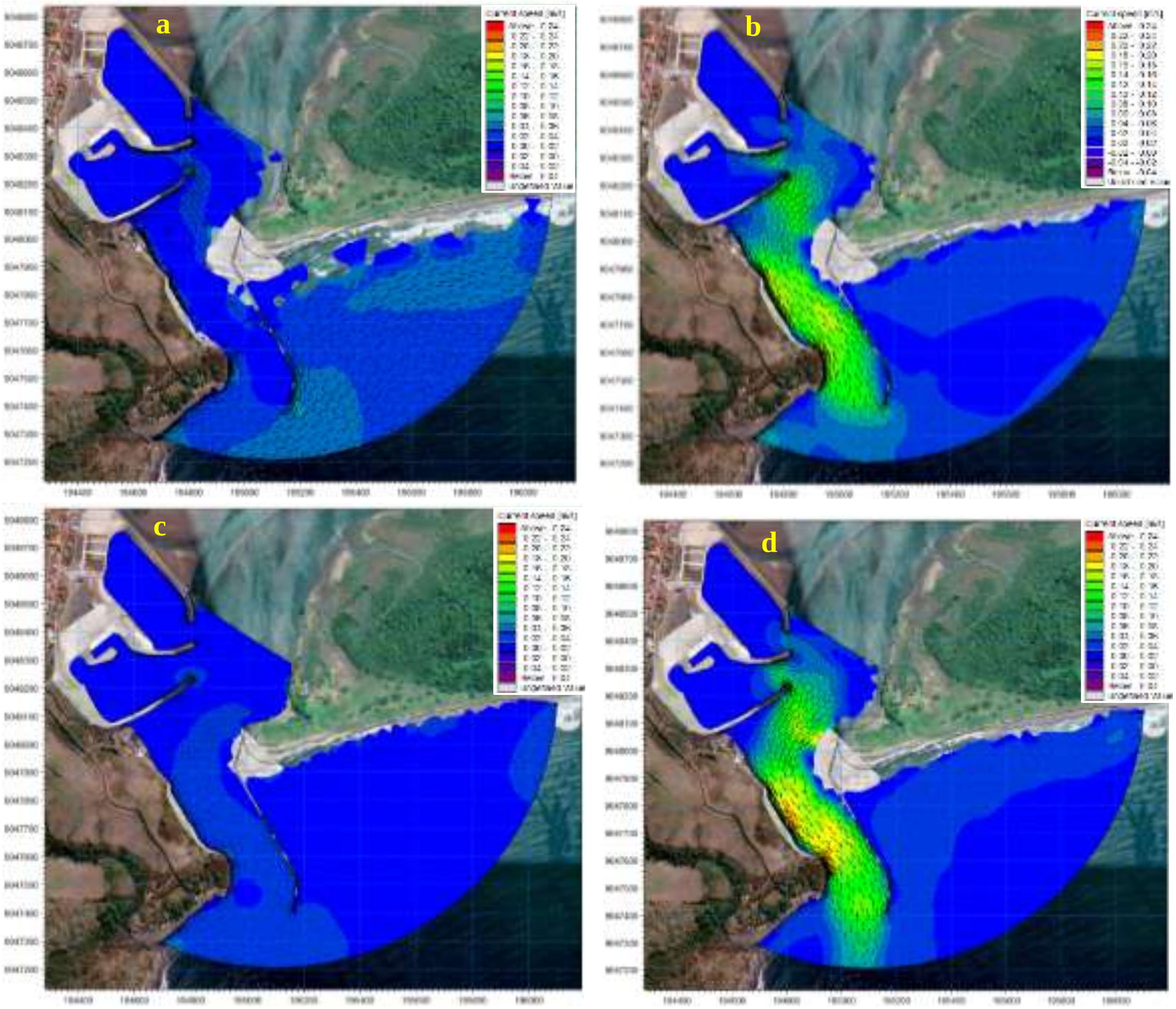

Figure 10. Tidal currents at (a) lowest ebb, (b) towards high tide, (c) highest tide, and (d) towards low tide.

3.6.2 Sediment Simulation Results After Dredging and Breakwater

The initial conditions on breakwater plan A, no sedimentation has been seen (Figure 14a). This condition is an existing condition before being exposed to tidal currents, so no sedimentation or erosion has been found. In the initial condition, the elevation value still follows the depth value during the survey. Elevation conditions on the estuary side of the river ranged from (-2.4)-3.2 m, the harbor area was 0 m, and the beach area ranged from 0-3.2 m.

Figure 14b is the final bed level condition after dredging. In the simulation results after dredging there is a difference in elevation than before dredging, especially in the harbor basin area. After dredging, there is no sedimentation or erosion phenomenon in the harbor basin. The final bed level condition in breakwater plan A, there is a change in elevation at the estuary, to the side of breakwater plan A. Sedimentation occurs on the side of the breakwater, while erosion occurs in the estuary area. Sedimentation that occurs on the near-land side of breakwater plan A has a bed level value ranging from 0-3.2m. The estuary area is affected by erosion with bed level elevations of -0.1 to -1.6 m.

After dredging, neither sedimentation nor erosion occurred in the harbor basin. In Figure 14c, the bed level change condition experienced erosion events that occurred at the mouth of the river and the east side of breakwater plan A. Sedimentation occurred on the west side of breakwater plan A and the mouth of the harbor pool. The estuary and shipping channel eroded up to -0.15 m, then on the east side of the breakwater there was also erosion up to -0.9m. On the west side of breakwater plan A, sedimentation up to 0.9 m occurred. Sedimentation also occurs at the mouth of the berth pond up to 0.3 m. Sedimentation occurs due to the influence of longshore currents that carry sediment along the coastline.

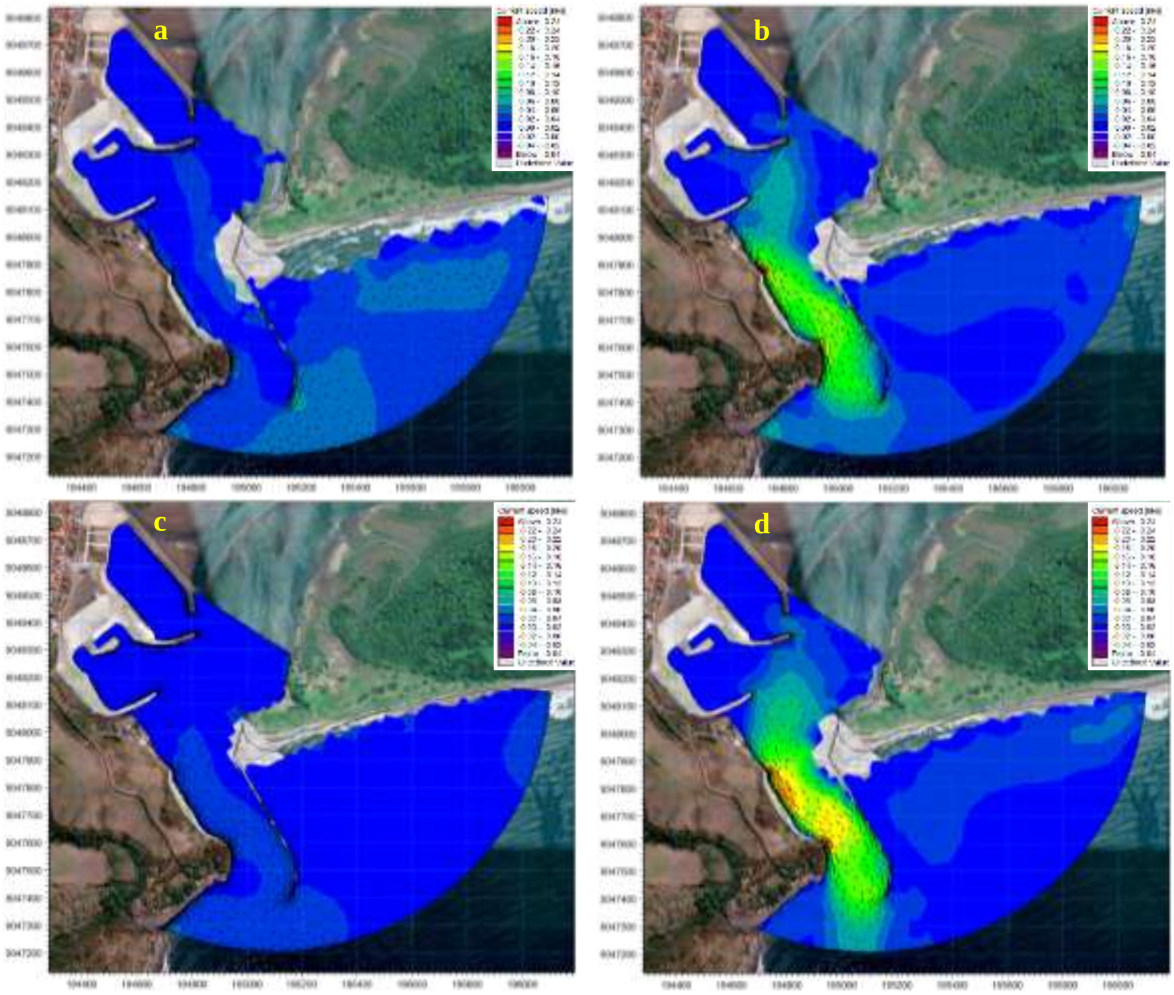

Figure 11. Tidal currents at (a) lowest ebb, (b) towards high tide, (c) highest tide, and (d) towards low tide.

Figure 15a shows that the initial bed level of breakwater plan B after dredging is not much different before dredging. The difference in elevation in the simulation after dredging is only in the harbor basin area which has a bed level value of 0 m. This condition is an existing condition before being exposed to tidal currents, so that no sedimentation or erosion has been found. Elevation conditions on the estuary side of the river ranged from 0-(-2.4) m, the harbor area was 0 m, and the beach area ranged from 0-3.2 m. The final bed level condition (Figure 15b) after dredging, sedimentation occurred on the west side of the breakwater and erosion on the east side of the breakwater. Erosion also occurred at the estuary with a bed level range of 0-(-2.4) m. Elevation changes on the west side of breakwater plan B ranged from 0.8-3.2 m, while on the east side of breakwater plan B erosion occurred with a bed level value of -1.6 m. The estuary area was also affected by erosion with a reduction in bed level to -1.6 m.

Simulation results on the condition of bed level change breakwater plan B (Figure 15c), sedimentation occurs on the west side of the breakwater, while in the harbor basin there is no sedimentation or erosion. Erosion occurs at the mouth of the river and the east side of the breakwater to the shoreline. Sedimentation that occurs on the west side of the breakwater has a bed level change value ranging from 0 to 0.75 m, while in the shipping channel there is sedimentation of up to 0.45m. Sedimentation also occurs on the breakwater side of the pond and the mouth of the berth pond ranging from 0.3-0.9 m. At the mouth of the river there is a decrease in bed level due to erosion in the range of 0 to -0.3 m, while along the coastline to the east side of the breakwater there is erosion ranging from -0.15 to -0.75 m. Erosion occurs due to rip currents that carry sediment along the shoreline to the sea.

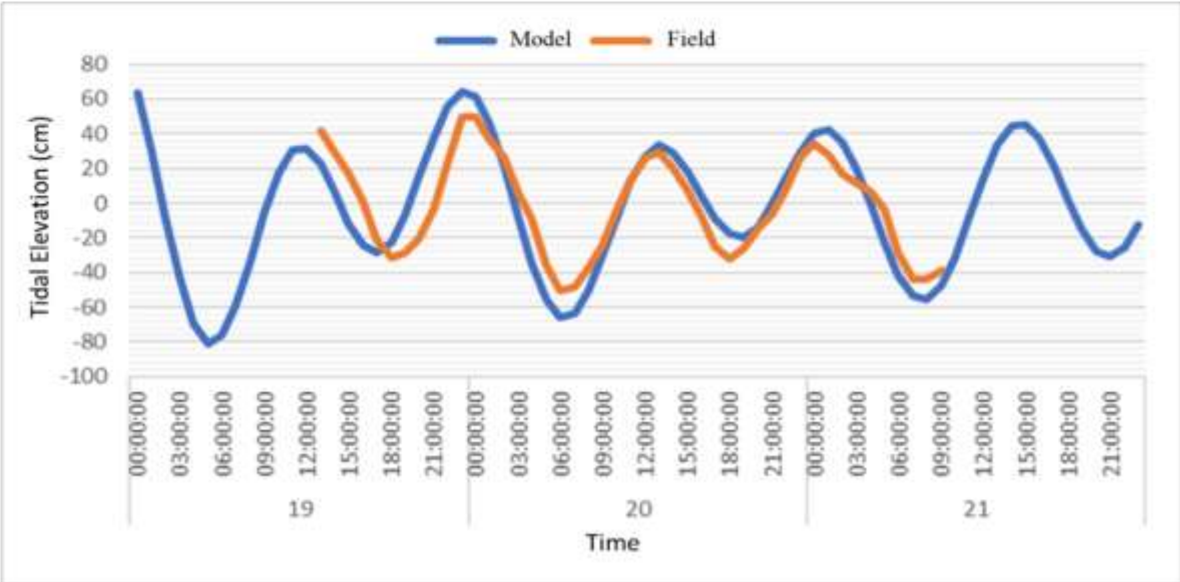

Figure 12. Validation of field tidal data with model results on November 19-21, 2023.

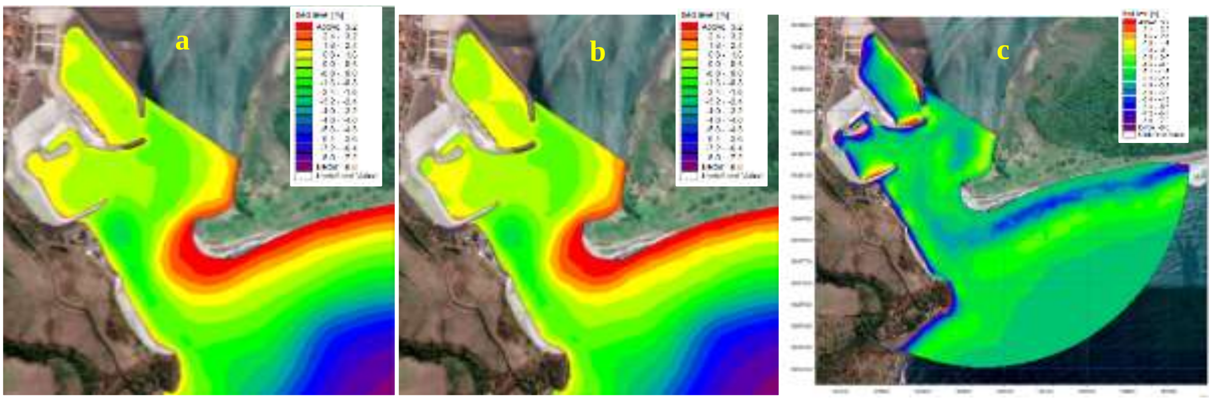

Figure 13. Bed level conditions (a) initial, (b) final, and (c) existing bed level change.

The initial bed level condition of breakwater plan C (Figure 16a) after dredging is not much different before dredging. The difference in elevation in the simulation after dredging is only in the harbor basin area which has a bed level value of 0 m. This condition is an existing condition before being exposed to tidal currents, so that no sedimentation or erosion has been found. In the initial condition, the elevation value still follows the depth value during the survey. Elevation conditions on the estuary side of the river ranged from 0 to -2.4 m, the harbor area was 0 m, and the beach area ranged from 0-3.2 m. Figure 16b with the final bed level condition after dredging, sedimentation occurs on the west side of the breakwater and erosion on the east side of the breakwater. The final condition of breakwater plan C and B only has a difference in elevation at the port door due to the short breakwater plan B. In breakwater plan C erosion occurs at the port door while in plan B sedimentation occurs. Erosion also occurs at the mouth of the river with a bed level range of 0 to -2.4 m. Elevation changes on the west side of breakwater plan B range from 0.8 to 3.2 m, while on the east side of breakwater plan B erosion occurs with a bed level value of -1.6 m. The estuary area was also affected by erosion with a reduction in bed level of up to -1.6 m.

Simulation results in Figure 16c breakwater plan C, no significant sedimentation or erosion was found in the estuary to the harbor basin. Sedimentation only occurs on the west side of the breakwater with a range of bed level changes up to 0.6 m and a small area. Erosion occurs in the shipping channel, estuary and east side of the breakwater.

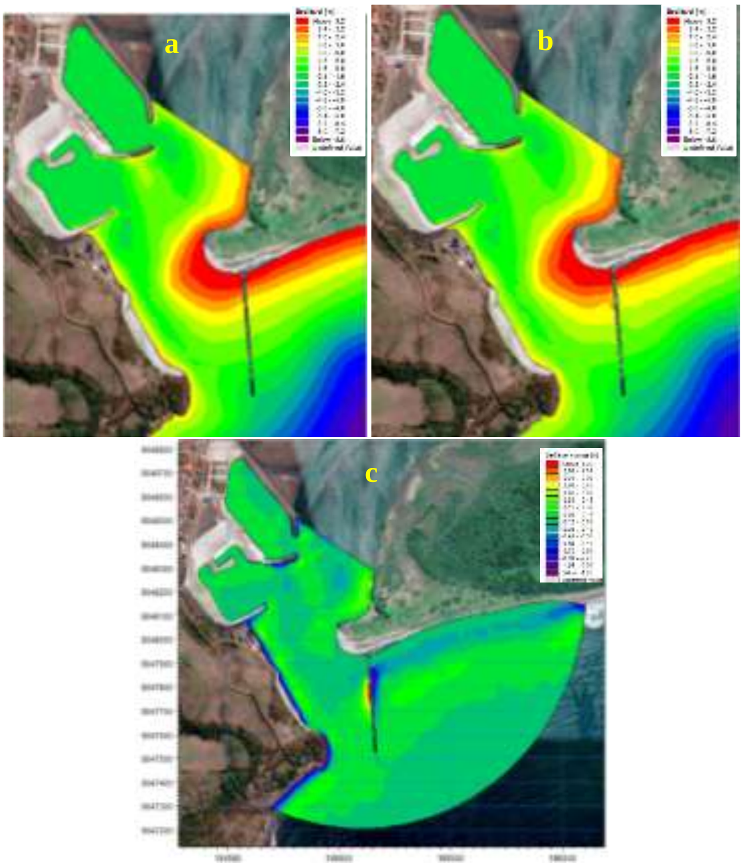

Figure 14. Breakwater plan A, bed level (a) initial, (b) final after dredging, and (c) bed level change after dredging.

In the shipping channel and estuary, erosion occurs up to -0.3 m, then on the east side of the breakwater there is also erosion up to -0.9 m. The shipping channel, the harbor door and the estuary are the most needed locations for ships to enter and exit the harbor safely. Erosion that occurs on the east side of the breakwater to along the shoreline is caused by rip currents that carry sediment to the sea.

In the simulation results after dredging, breakwater plan C is considered the most effective than plans A and B. This is because the shape of breakwater plan C is able to overcome the influence of sedimentation in the Grajagan harbor basin. Breakwater plan B is less effective because of the presence of a breakwater building in the harbor basin which results in sediment trapped around the breakwater of the plan B harbor basin. Layout breakwater plan A is less effective because the estuary door is still wide which can make sediment enter the harbor basin directly.

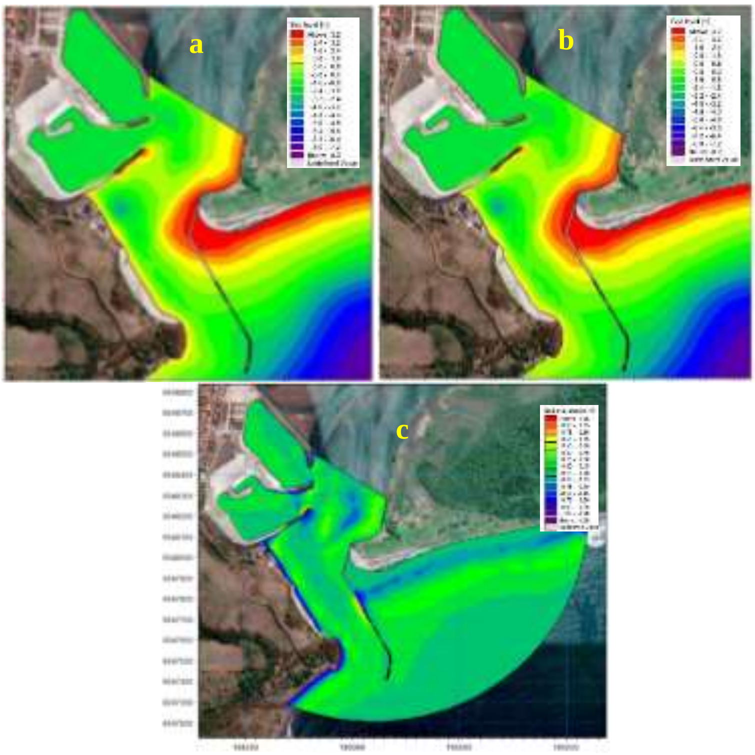

Figure 15. Breakwater plan B conditions (a) initial, (b) final, and (c) bed level change after dredging.

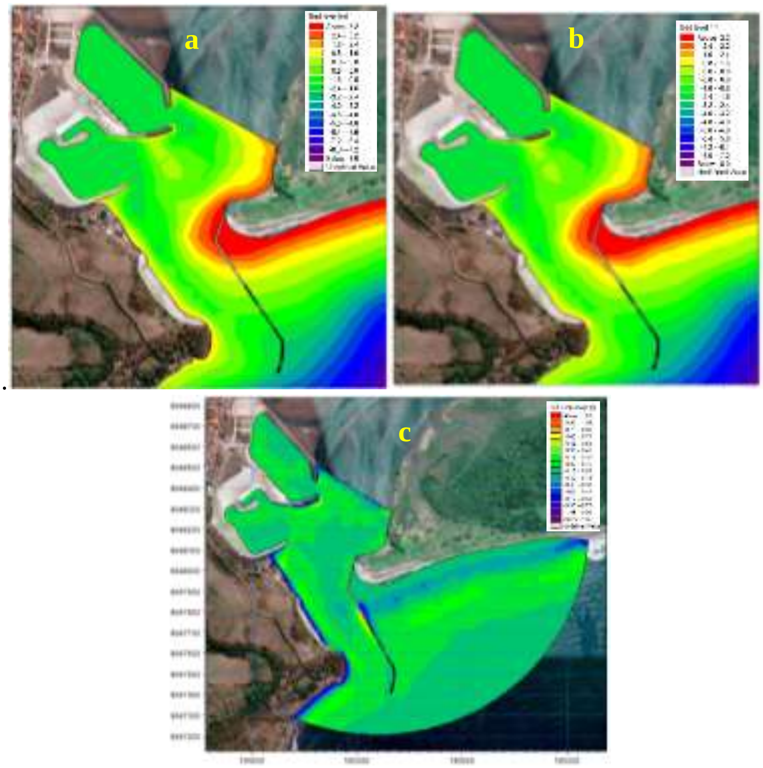

Figure 16. Breakwater plan C conditions (a) initial, (b) final, and (c) bed level change after dredging.

4. Conclusion

Prior to the breakwater's construction, the harbor basin area witnessed a more pronounced accumulation of sediment compared to the post-construction period. Pre-breakwater construction, the harbor basin area, including the harbor basin door, experienced sedimentation reaching 0.6 meters. The east side of the river witnessed sedimentation of up to 0.3 meters, while erosion ranging from -0.15 to -0.1 meters occurred on the west side of the estuary.

After the construction of breakwater layouts A, B, C, and also dredging in the harbor basin, the following simulation results were obtained: (a) Layout breakwater plan A in the harbor basin, no sedimentation occurs. On the west side of breakwater plan A, sedimentation up to 0.9 m occurs, while the east side of breakwater plan A erosion up to -0.9 m occurs. At the mouth of the harbor basin, sedimentation of up to 0.3 m occurred. The shipping channel erodes up to -0.15 m, (b) Layout breakwater plan B does not occur sedimentation in the berth pond, but sedimentation occurs on the west side of the breakwater up to 0.75m. In the shipping channel there is sedimentation up to 0.45 m. The mouth of the berth pond and the breakwater side of the pond occur sedimentation of 0.3 to 0.9 m. Layout breakwater plan C sedimentation only occurs on the west side of the breakwater up to 0.6 m, while in the shipping channel and the berth pool neither sedimentation nor erosion occurs. Based on the simulation results of breakwater layouts A, B, and C, breakwater layout C emerges as the most optimal solution for the Grajagan Beach Fishing Port in Banyuwangi Regency. Layout C demonstrates superior efficiency in maintaining the harbor basin compared to layouts A and B.

Acknowledgements

The author wishes to express gratitude to Hang Tuah University for their support in the completion of this research. Additionally, the author would like to thank the relevant parties who provided the opportunity to conduct field observations in Grajagan Waters, Banyuwangi.

Reference

[1] Bachtiar H, Setiantoro H E, Prasetyo A, Eliasta L, and Putriasi A E. 2020. Pendekatan model komputasi untuk penanggulangan sedimentasi pelabuhan akibat pengaruh muara sungai studi kasus Pelabuhan Tanjung Mas Semarang. *Jurnal Teknik hidraulik*, **11** (2), pp. 119-134.

[2] Gemilang R I A, and Kurniawan Y N. 2016. Efektifitas redaman energi gelombang akibat adanya *breakwater* terapung ditinjau dari model fisik dan studi numerik. *Jurnal online institut teknologi nasional*, **2** (3), pp. 147-157.

[3] Gemilang W A, Rahmawan G A, and Wisha U J. 2017. Kualitas perairan Teluk Ambon Dalam berdasarkan parameter fisika dan kimia pada musim peralihan I. *EnviroScienteae*, **13** (1), pp. 79-90.

[4] Harsono G, and Hartoyo D. 2018. *Dasar-dasar survei hidro-oseanografi*. Bogor: IPB Press.

[5] Izzati A. 2018. Redesign bangunan pengaman pantai sebagai alur masuk pelayaran Pelabuhan Perikanan Jember. Institut Teknologi Surabaya.

[6] Laksono FAT, Borzì L, Distefano S, Di Stefano A, and Kovács, J. (2022). Shoreline prediction modelling as a base tool for coastal management: The Catania plain case study (Italy). *Journal of Marine Science and Engineering*, **10**(12), 1988.

[7] Miranda NA, Bintoro RS, and Prasita VD. 2023. The pattern of coastline changes and wave modelling around the expansion of PPI Popoh Tulung Agung, East Java. *Maritime Technology and Research*, **5**(4): 262926.

[8] Nofrizal, and Istijono B. 2018. Pengaruh transport sedimen dan curah hujan tahunan terhadap penambahan volume sedimen di muara Sungai Batang Arau. *ACE Confrence* **5**, pp. 344-353.

[9] Nurisman N, and Taringan T A B. 2020. Model fisik pengaruh submerged *breakwater* terhadap gelombang datang. *Jurnal penelitian sains*, **22** (2), pp. 95-98.

[10] Purnama E A, Hariadi, and Saputro E. 2015. Pengaruh arus, pasang surut dan debit sungai terhadap distribusi sedimen tersuspensi di Perairan Muara Sungai Ciberes, Cirebon. *Jurnal oseanografi*, **4** (1), pp.74-84.

[11] Ratnasari K D, Dermawan D, and Rizal M. C. 2018. Studi karakteristik lumpur intake perusahaan pembangkit listrik. *Proceeding on waste treatment technology*, **1** (1), pp. 171-176.

[12] Roswaty M R M, and Purnomo P W. 2014. Tingkat sedimentasi di muara Sungai Wudung Kecamatan Wedung, Demak. *Maquares*, **3** (2), pp.129-137.

[13] Saputra H, Subardjo P, and Saputro S. 2013. Studi pola sebaran sedimen dasar akibat arus sepanjang pantai di sekitar pemecah gelombang Pantai Kuta Bali. *Jurnal oseanografi*, **2**(2), pp. 161-170.

[14] Simatupang C M, Surbakti H, and Agussalim A. 2016. Analisis data arus di perairan muara Sungai Banyuasin Provinsi Sumatera Selatan. *Maspari journal*, **8** (1), pp.15-24.

[15] Syahputra T R, and Rahma, E. A. 2023. Karakteristik pasang surut air laut di Periran Belawan menggunakan metode admiralty. *Jurnal ilmu kelautan*, **5** (1), pp. 7-16.

[16] Syahza A. 2021. *Buku Metodologi Penelitian, Edisi Revisi Tahun 2021*. Pekanbaru: UR Press.

[17] Triatmodjo B. 2016. *Teknik pantai*. Yogyakarta: BETA.

[18] Warsidah, Risko, Saputra D W, Muliadi, Zibar Z, and Susiati H. 2021. Sebaran sedimen berdasarkan analisis parameter ukuran butir di muara Sungai Sambas Kalimantan Barat. *Jurnal geologi kelautan*, **19** (2), pp.61-71.

[19] Wiyono R U A, Fadhila A, Ma A R M, Halik G, Widiarti W Y, and Hidayah. 2023. Effect of breakwater layout on waves at Puger Beach Jember with Delft3D modelling. *E3S Wb of Conferences*.